


**Rescattering time-energy analysis of high-order above-threshold ionization in few-cycle laser fields**Li Guo,<sup>1,\*</sup> Shi Chen<sup>2</sup>,,<sup>2</sup> Mingqing Liu,<sup>3</sup> Zheng Shu,<sup>3</sup> Shilin Hu,<sup>4</sup> Ronghua Lu,<sup>1</sup> Shensheng Han,<sup>1</sup> and Jing Chen<sup>3,5,†</sup><sup>1</sup>*Key Laboratory for Quantum Optics and Center for Cold Atom Physics, Shanghai Institute of Optics and Fine Mechanics, Chinese Academy of Sciences, Shanghai 201800, China*<sup>2</sup>*HEDPS, Center for Applied Physics and Technology, Collaborative Innovation Center of IFSA, Peking University, Beijing 100084, China*<sup>3</sup>*Institute of Applied Physics and Computational Mathematics, P.O. Box 8009, Beijing 100088, China*<sup>4</sup>*Laboratory of Quantum Engineering and Quantum Metrology, School of Physics and Astronomy, Sun Yat-Sen University (Zhuhai Campus), Zhuhai 519082, China*<sup>5</sup>*Center for Advanced Material Diagnostic Technology, College of Engineering Physics, Shenzhen Technology University, Shenzhen 518118, China*

(Received 23 October 2019; accepted 25 February 2020; published 27 March 2020)

A Wigner distributionlike function based on the improved strong-field approximation theory is proposed to calculate the rescattering time-energy distribution (RTED) of high-energy photoelectrons of atomic above-threshold ionization process in few-cycle laser fields with different frequencies. The RTED shows bell-like stripes and the outermost stripe is compared with semiclassical results given by the simple-man model with consideration of different positions of tunnel exit and different initial longitudinal momenta. Analysis indicates the existence of the tunnel exit. However, though it shifts farther away from the core with decreasing frequency, the position of the tunnel exit is significantly less than the prediction by adiabatic theory even for the low-frequency case which is well in the tunneling regime. Our results also imply that the effect of the tunnel exit is more important than that of the initial longitudinal momentum at the tunnel exit for the backward-scattering electrons. Moreover, the inner stripe structures in the RTED are attributed to interference between electrons with the same final energy emitted at different ionization times.

DOI: [10.1103/PhysRevA.101.033415](https://doi.org/10.1103/PhysRevA.101.033415)**I. INTRODUCTION**

An atom will be ionized when it is exposed to an external static electric field which can be understood by a tunneling process: The bound electron tunnels through the potential barrier formed by the combination of the Coulomb and external fields [1]. With this perspective in mind, the above-threshold ionization (ATI) process [2] of atoms and molecules in intense laser fields with long wavelength, through an intrinsic multiphoton process, can be described by a simple-man picture: The electron tunnels through the barrier and then moves in the laser field (or in the presence of both Coulomb and laser fields) [3,4]. Moreover, the electron can be driven back by the laser field to revisit the core and, subsequently, can have three different consequences. Elastic collision, inelastic collision, and recombination give rise to the high-energy plateau of the energy spectrum [5], nonsequential double ionization (NSDI) [6,7], and the plateau of high-order harmonic generation (HHG) [8,9], respectively, which is usually called the standard three-step model [10,11]. This semiclassical model, which is generally accepted to be suitable in the adiabatic regime, with further development to take into account the tunnel exit of  $-I_p/E(t)$  (here  $I_p$  is the ionization potential of the atom and  $E(t)$  is the electric field at tunneling moment  $t$ ) and zero initial

longitudinal momentum at the tunnel exit has successfully explained various phenomena [12–16].

Recently, some experiments and calculations find that agreement between the experiments and semiclassical calculations cannot be achieved unless some **nonadiabatic effects**, e.g., modified tunneling exit [17–19] and nonzero initial longitudinal momentum [20–25], are considered. In the three-step model, the tunnel exit and the initial longitudinal momentum are important quantities which affect the energy of the electron when the electron returns to the core, and thus they have noticeable impacts on the energy spectrum, NSDI, and HHG processes. In turn, these phenomena can be used to investigate the nonadiabatic effect and further improve the semiclassical model by comparing the results between the experiments (or quantum calculations) and the semiclassical model. However, since both experiment and quantum calculation can only give the final kinetic energy spectrum (or momentum spectrum) detected by the detector, it is hard to extract information, e.g., the maximal energy that an electron can achieve in the laser field and the corresponding rescattering moment, to compare with the calculation of the semiclassical model to investigate the nonadiabatic effects.

Previously, we proposed a Wigner distributionlike (WDL) function based on the strong-field approximation (SFA) theory [26], with which we have studied the time-related distribution of the photoelectron in the ATI process [26–28]. In this paper, we propose a WDL function based on the improved strong-field approximation (ISFA) (namely, the second term of the  $S$ -matrix expansion) [29–31]. It allows us to obtain

\*guoli@siom.ac.cn

†chen\_jing@iapcm.ac.cn

the final energy as a function of the rescattering time, i.e., rescattering time-energy distribution (RTED). By comparing with the semiclassical results, we can check the validity of the semiclassical picture and study the nonadiabatic effects caused by the tunnel exit and the initial longitudinal momentum explicitly.

## II. THEORY METHOD

In order to avoid repetition, here we only present derivation of the formula briefly (see Refs. [26,28] for more details). The rescattering term of the  $S$ -matrix expansion is given in the length gauge [29,30]:

$$\begin{aligned} S_{\text{fi}}^{(1)} &= \int_{-\infty}^{\infty} dt \int_{-\infty}^t dt_0 \int d\mathbf{k} \langle \chi_{\mathbf{p}}(t) | V | \chi_{\mathbf{k}}(t) \rangle \langle \chi_{\mathbf{k}}(t_0) | \\ &\quad \times \mathbf{r} \cdot \mathbf{E}(t_0) | \varphi_i(t_0) \rangle \\ &= \frac{1}{\sqrt{2\pi}} \int_{-\infty}^{\infty} dt S' e^{i\frac{p^2}{2}t}. \end{aligned} \quad (1)$$

Here,  $V$  is the Coulomb potential,  $\mathbf{E}(t_0)$  is the electric field of the laser pulse, and  $|\varphi_i(t)\rangle = |\varphi_0\rangle e^{iI_p t}$  is the atomic ground state. The  $|\chi_{\mathbf{q}}(t)\rangle$  is the Volkov wave function with the canonical momentum  $\mathbf{q}$ , which has the form

$$|\chi_{\mathbf{q}}(t)\rangle = |\mathbf{q} + \mathbf{A}(t)\rangle \exp \left[ -i \int_{-\infty}^t \frac{[\mathbf{q} + \mathbf{A}(\tau)]^2}{2} d\tau \right], \quad (2)$$

where  $\mathbf{A}(t) = -\int \mathbf{E}(t)dt$  is the vector potential of the laser pulse. Here,  $S'$  is given by

$$\begin{aligned} S' &= \sqrt{2\pi} \int_{-\infty}^t dt_0 \int d\mathbf{k} \langle \mathbf{p} | V | \mathbf{k} \rangle \langle \mathbf{k} + \mathbf{A}(t_0) | \mathbf{r} \cdot \mathbf{E}(t_0) | \varphi_i \rangle \\ &\quad \times \exp \left\{ i \int_{-\infty}^t \left[ \mathbf{p} \cdot \mathbf{A}(\tau) + \frac{\mathbf{A}^2(\tau)}{2} \right] d\tau \right\} \\ &\quad \times \exp \left\{ -i \int_{t_0}^t \frac{[\mathbf{k} + \mathbf{A}(\tau)]^2}{2} d\tau + iI_p t_0 \right\}, \end{aligned} \quad (3)$$

where  $\mathbf{p}$  is the final kinetic momentum and  $\mathbf{k}$  is the canonical momentum.

The WDL function based on the ISFA theory in a two-dimensional system is given by

$$f\left(t, \frac{p^2}{2}, \Theta\right) = \frac{1}{\pi} \int_{-\infty}^{\infty} S'^*(t+t', \Theta) S'(t-t', \Theta) e^{-2i\frac{p^2}{2}t'} dt', \quad (4)$$

where  $\Theta$  is the electron emission angle with respect to one coordinate axis ( $x$  axis in this paper).

$S'$  is evaluated by solving the integrals over the ionization time  $t_0$  and the intermediate canonical momentum  $\mathbf{k}$ . Here, we adopt the saddle-point method to solve the integrals over  $t_0$  and  $\mathbf{k}$ . The remaining time variables, i.e., the rescattering time, in Eq. (4) are numerically calculated. The integrals of all variables in Eq. (1) are correspondingly performed in the same way as mentioned above. The saddle-point equations are satisfied for the variables  $t_0$  and  $\mathbf{k}$  as follows:

$$\frac{[\mathbf{k} + \mathbf{A}(t_0)]^2}{2} + I_p = 0; \quad \mathbf{k} = - \int_{t_0}^t d\tau \mathbf{A}(\tau) / (t - t_0). \quad (5)$$

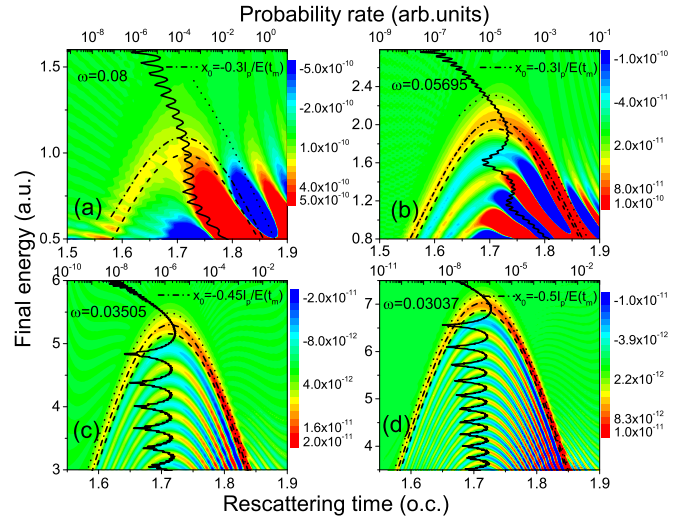


FIG. 1. The rescattering time-energy distribution for four different frequencies obtained by Eq. (4) with  $\omega = 0.08$  a.u. (a), 0.05695 a.u. (b), 0.03505 a.u. (c), and 0.03037 a.u. (d). The solid lines are the energy spectra. The other lines are the semiclassical curves without considering the initial longitudinal momentum for different tunnel exits:  $x_0 = 0$  (dashed lines),  $x_0 = -I_p/E(t_m)$  (dotted lines), and other values marked in each panel (dashed dotted lines) (see text).

According to the characteristic of the WDL function [26,28], the energy spectrum along the emission angle  $\Theta$  can be obtained by integrating Eq. (4) over time  $t$  as follows:

$$W\left(\frac{p^2}{2}, \Theta\right) = \int f\left(t, \frac{p^2}{2}, \Theta\right) dt. \quad (6)$$

It is noteworthy that the energy spectrum obtained by Eq. (6) is exactly the same as that calculated directly by the ISFA theory, which is strictly proved in Refs. [26,28].

The vector potential of a linearly polarized laser field is adopted as follows:

$$\mathbf{A}(t) = -\frac{E_0}{\omega} \sin^2 \left[ \frac{\omega t}{2n} \right] \cos(\omega t + \varphi) \mathbf{e}_x, \quad (7)$$

where  $E_0$  is the peak laser field strength,  $\omega$  is the laser frequency,  $n$  is the number of optical cycles (o.c.) contained in the laser pulse,  $\varphi$  is the initial carrier-envelope phase, and  $\mathbf{e}_x$  is the unit vector along the  $x$  axis.

In this paper, we only focus on the electrons emitted from hydrogen atoms in the laser polarization direction ( $\Theta = 0$ ) in intense laser pulses with a duration of 3 o.c. for simplicity. The peak intensity of the laser pulse is  $1 \times 10^{14}$  W/cm<sup>2</sup>. Atomic units (a.u.) are used unless otherwise indicated.

## III. RESULTS AND DISCUSSIONS

Figure 1 shows the rescattering time-energy distributions of photoelectrons at the emission angle  $\Theta = 0$  calculated by Eq. (4) for four different frequencies. The corresponding energy spectra (solid lines) calculated by the ISFA theory are also given in Fig. 1. The corresponding Keldysh parameters ( $\gamma = \omega\sqrt{2I_p}/E_0$ ) are 1.495, 1.064, 0.655, and 0.568 for four frequencies, respectively. As can be seen in Fig. 1, more and more bell-like stripes gradually appear in the

rescattering time-energy distribution with decreasing laser frequency. One can find that, except for the highest-frequency case, the positions of the peaks in the energy spectrum correspond to the peaks of the bell-like stripes. It is well-known that these peaks in the energy spectrum can be attributed to the interference between electrons with long and short orbits [29,32], indicating that these stripes in the RTED are also due to interference between electrons emitted at different moments but possessing the same final kinetic energy.

Moreover, we give the final kinetic energy as a function of the rescattering time calculated by the semiclassical method (i.e., simple-man method) with different tunnel exits  $x_0$  in Fig. 1. According to the simple-man theory, an electron after tunnelling classically moves in the laser field and interacts with the core by backscattering when it returns to the core. For the semiclassical calculation, we first assume that the initial longitudinal momentum at the tunnel exit is zero. (The initial transverse momentum is not considered because the electrons only ejected at  $\Theta = 0$  are investigated in this paper.) Thus, the semiclassical result is only dependent on the position of the tunnel exit  $x_0$ . As shown in Fig. 1, the larger the value of  $x_0$  is, the higher is the electron energy for a given frequency. As can be seen in Fig. 1, the semiclassical curves are more and more consistent with the outermost stripes with decreasing frequency. For  $\omega = 0.08$  a.u., which is in the multiphoton regime and no clear cutoff can be seen in the energy spectrum, the semiclassical curves with smaller tunnel exits ( $x_0 = 0$  and  $-0.3I_p/E(t_m)$ , where  $t_m$  is the ionization time in the semiclassical calculations) roughly correspond to the stripe in the RTED, but the curve of  $x_0 = -I_p/E(t_m)$  is far beyond the region of the stripe. For  $\omega = 0.05695$  a.u., which is approximately in the adiabatic regime ( $\gamma \sim 1$ ), the semiclassical curve of  $x_0 = 0$  corresponds to the lower edge of the outermost stripe in the RTED while the curve of  $x_0 = -I_p/E(t_m)$  still deviates from the stripe noticeably. When the frequency decreases further into the tunneling regime, i.e.,  $\omega = 0.03505$  and  $0.03037$  a.u., the semiclassical curves of  $x_0 = 0$  and  $-I_p/E(t_m)$  correspond to the lower and upper edges of the outermost stripes in the RTED, indicating that the semiclassical picture is valid in the tunneling regime. It is noted that the maximal energy an electron can achieve in the ionization process is difficult to be identified from the quantum calculations due to the continuity of the energy spectrum. Therefore, we take the central maxima of the outermost stripe as a criterion. We scan the tunnel exit and choose the value with which the semiclassical curve agrees well with the central maximal of the outermost stripe. The chosen tunnel exit is denoted by  $x_a$ . The values of  $x_a$  are  $-0.5I_p/E(t_m)$ ,  $-0.45I_p/E(t_m)$ , and  $-0.3I_p/E(t_m)$  for  $\omega = 0.03037$ ,  $0.03505$ , and  $0.05695$  a.u., respectively, as exhibited in Fig. 1. This result shows that the tunnel exit is getting close to the core with increasing frequency when the initial longitudinal momentum at the tunnel exit is neglected. It is consistent with the understanding that the tunnel exit becomes smaller in the nonadiabatic regime due to an increase of the electron energy under the potential barrier before tunneling out [17,19].

We further consider the initial longitudinal momentum  $v_x$  of the photoelectron at the tunnel exit in the semiclassical calculations. Here we consider  $\omega = 0.05695$  a.u. as an example. The values of  $v_x$  are chosen as  $-0.2$ ,  $0$ ,  $0.2$ , and

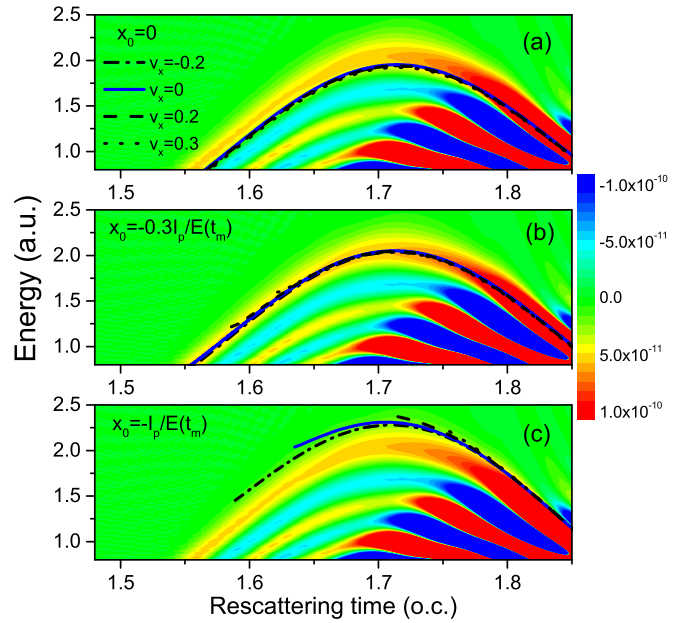


FIG. 2. The semiclassical results with different initial longitudinal momenta  $v_x$  and tunnel exits  $x_0$  calculated by the simple-man method for the case of  $\omega = 0.05695$  a.u. The tunnel exits are  $x_0 = 0$  (a),  $-0.3I_p/E(t_m)$  (b), and  $-I_p/E(t_m)$  (c), respectively. The RTED is also given in each panel for comparison.

0.3 a.u. Figures 2(a)–2(c) show the semiclassical results with different values of  $v_x$  for three fixed tunnel exits of  $x_0 = 0$ ,  $-0.3I_p/E(t_m)$ , and  $-I_p/E(t_m)$ , respectively. For comparison, the RTED for  $\omega = 0.05695$  a.u. is also plotted in Fig. 2. For all three cases, the semiclassical curve with nonzero  $v_x$  only shifts slightly with respect to that of  $v_x = 0$ . From Fig. 2, it can be clearly seen that for the two cases of  $x_0 = 0$  and  $-I_p/E(t_m)$ , the semiclassical curves cannot be in accordance with the central maxima of the outermost stripe, no matter what the value of the initial longitudinal momentum is. Only when one appropriate tunnel exit is considered can the agreement be achieved. This means that the semiclassical curve mainly depends on  $x_0$ . Moreover,  $v_x$  can change the trajectory of the electron, which is more obvious for large values of  $x_0$  [see Figs. 2(b) and 2(c)]. It is easy to understand that the larger the value of  $v_x$ , the later the electron returns to the core. In addition, the value of  $v_x$  has a significant impact on the ionization time for a specific rescattering time and thus affects the ionization rate, i.e., the weight of the trajectory. It is worthwhile mentioning that Li *et al.* show that the longitudinal momentum becomes larger with increasing final kinetic energy [25], which is different from our result given in this paper. The former is more consistent with the case of direct electrons obtained by the WDL based on the SFA theory (see the comparison of ionization stripe and the semiclassical curve in Figs. 2(e) and 2(f) of Ref. [27]). Therefore, this difference may be attributed to different scattering processes of electrons; in Ref. [25], the authors focus on the forward-scattering electrons, while we concentrate on the backward-scattering electrons.

Next, we discuss the origin of the stripes in the RTED by considering the case of  $\omega = 0.03505$  a.u. as an example. In the process of the saddle-point calculation, for a given

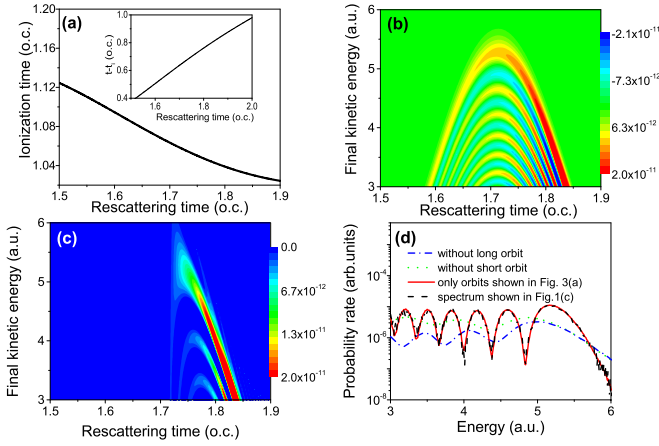


FIG. 3. (a) The ionization time  $t_i$  as a function of the rescattering time calculated by the saddle-point method. The difference between the rescattering and ionization times are given in the inset. (b) The RTED for electrons emitted at the ionization time range shown in panel (a). (c) The RTED for electrons of only long orbits. (d) The energy spectra calculated by the ISFA theory for electrons of only long (dotted line), only short (dashed dotted line), and long and short (solid line) orbits and the total energy spectrum shown in Fig. 1(c) (dashed line), respectively.

rescattering time  $t_r$ , we can determine the ionization time  $t_0$  by solving Eq. (5), which is independent of the final electron momentum  $\mathbf{p}$ . Generally,  $t_0$  is a complex number. The real part of  $t_0$  is usually considered as the ionization time of the electron in real time, which is labeled by  $t_i = \text{real}[t_0]$ . Therefore, we can obtain the ionization time  $t_i$  as a function of the rescattering time  $t_r$ , as shown in Fig. 3(a) (another range of ionization time is not shown here due to its negligible contribution to the high-energy electrons).

As shown in Fig. 3(a), the earlier the electron is ionized, the later it scatters with the core. The difference between the ionization and rescattering times increases with the rescattering time, which is exhibited in the inset of Fig. 3(a). In Fig. 3(b), the rescattering time-energy distribution calculated by Eq. (4) is depicted for the electrons only emitted in the ionization time range shown in Fig. 3(a). A series of regular stripes which are almost identical to those shown in Fig. 1(c) is presented in Fig. 3(b). The comparison between the outermost stripe and the semiclassical curve as shown in Fig. 1(c), together with the ionization time range shown in Fig. 3(a), indicates that the outermost stripe in Figs. 1(c) and 3(b) results from the backward-scattering electrons emitted at the ionization time range shown in Fig. 3(a). The rising and falling edges of the outermost stripe correspond to the short and long orbits of electrons, respectively. The other stripes in Fig. 3(b), namely, the inner stripes, result from the constructive interference between electrons with the same final energy emitted at different ionization times, which have no classical correspondences. It is important to point out that interference mentioned above is not restricted to the interference between the long and short orbits. This can be demonstrated from the rescattering time-energy distribution calculated without short orbit considered as shown in Fig. 3(c).

The interference stripes still exist in the rescattering time-energy distribution although the interference patterns of the

stripes are changed due to the absence of the short orbit [see Fig. 3(c)]. The energy spectra calculated by the ISFA theory without long or short orbits are also given in Fig. 3(d) and exhibit obvious oscillation due to the interference.

However, this interference is absent in the calculation in which the integrals of all variables in Eqs. (1) and (4) are calculated by the saddle-point method (below this is called the standard saddle-point method in order to be distinguished from the method used in our paper.) In the standard saddle-point method, when the values of the rescattering time  $t_r$  and the ionization time  $t_0$  are fixed, the momentum  $p$  is also fixed (denoted by  $p_s$ ). Hence there are two exact short and long trajectories corresponding to the rising and falling edges of the outermost stripe in the RTED, which are generally denoted by  $t_r$ ,  $t_0$ , and  $p_s$ . The interference can only occur between short and long trajectories. In our calculations, however, the momentum  $p$  can be any values for fixed values of  $t_r$  and  $t_0$  due to the independence of the saddle-point equations, Eqs. (5), on the momentum. This means that besides the two exact trajectories given by the standard saddle-point method, the ionization rate with  $p \neq p_s$  is also nonzero. Therefore, when the short trajectory is dropped, the interference also remains.

In addition, according to the feature of the WDL function, the interference between long and short orbits mainly locates at about the symmetry axis of the long and short orbits, namely, the central axis of the bell stripes. From Fig. 1, one can find that the maxima (minima) of the energy spectra approximately correspond to the peaks of the constructive (destructive) stripes. This indicates that the multippeak structure in the energy spectrum *mainly* comes from the interference between the long and short orbits, which is consistent with the previous understanding.

#### IV. CONCLUSION

In conclusion, the rescattering time-energy distributions calculated by the WDL function based on the ISFA are compared with the semiclassical results given by the simple-man model with different tunnel exits and initial longitudinal momenta at the tunnel exit, which exhibit that the semiclassical model becomes gradually valid with decreasing frequency. Comparison shows that only when one specific tunnel exit is considered can the semiclassical result agree well with the outermost stripe in the RTED for a given frequency, indicating the existence of the tunnel exit. Moreover, it is found that the obtained tunnel exit shifts away from the core with decreasing frequency; however, it is significantly closer to the core than the prediction of the adiabatic theory even for the low-frequency case. Meanwhile, our results also show that the initial longitudinal momentum at the tunnel exit has negligible impact on the semiclassical curves for the backward-scattering case and changes only the weight of the trajectory. Finally, the origins of the stripes in the RTED are given: The outermost stripe comes from the electrons corresponding to the first return trajectory in the semiclassical model, and the other regular stripes result from the constructive interference between electrons with the same final energy emitted at different ionization times, which is not restricted to the interference between long and short orbits.



## ACKNOWLEDGMENTS

This work was partially supported by the National Key Program for S&T Research and Development (Grants No.

2019YFA0307700 and No. 2016YFA0401100), the NNSFC (Grants No. 11774361, No. 11775286, No. 11425414, and No. 11804405), and the Open Fund of the State Key Laboratory of High Field Laser Physics (SIOM).

- 
- [1] L. D. Landau and E. M. Lifshitz, *Quantum Mechanics* (Pergamon, New York, 1977).
  - [2] P. Agostini, F. Fabre, G. Mainfray, G. Petite, and N. K. Rahman, *Phys. Rev. Lett.* **42**, 1127 (1979).
  - [3] L. V. Keldysh, *Sov. Phys. JETP*, **20**, 1307 (1965).
  - [4] H. B. Heuvell, van Linden van den, and H. G. Muller, in *Multiphoton Processes*, edited by S. J. Smith and P. L. Knight (Cambridge University, Cambridge, England, 1988).
  - [5] G. G. Paulus, W. Nicklich, H. Xu, P. Lambropoulos, and H. Walther, *Phys. Rev. Lett.* **72**, 2851 (1994).
  - [6] A. L'Huillier, L. A. Lompre, G. Mainfray, and C. Manus, *Phys. Rev. Lett.* **48**, 1814 (1982).
  - [7] A. L'Huillier, L. A. Lompre, G. Mainfray, and C. Manus, *J. Phys. B: At. Mol. Phys.* **16**, 1363 (1983).
  - [8] A. McPherson, G. Gibson, H. Jara, U. Johann, T. S. Luk, I. A. McIntyre, K. Boyer, and C. K. Rhodes, *J. Opt. Soc. Am. B* **4**, 595 (1987).
  - [9] M. Ferray, A. L'Huillier, X. F. Li, L. A. Lompre, G. Mainfray, and C. Manus, *J. Phys. B: At., Mol. Opt. Phys.* **21**, L31 (1988).
  - [10] K. J. Schafer, B. Yang, L. F. DiMauro, and K. C. Kulander, *Phys. Rev. Lett.* **70**, 1599 (1993).
  - [11] P. B. Corkum, *Phys. Rev. Lett.* **71**, 1994 (1993).
  - [12] M. Lewenstein, P. Balcou, M. Y. Ivanov, A. L'Huillier, and P. B. Corkum, *Phys. Rev. A* **49**, 2117 (1994).
  - [13] X. L. Hao, G. Q. Wang, X. Y. Jia, W. D. Li, J. Liu, and J. Chen, *Phys. Rev. A* **80**, 023408 (2009).
  - [14] X. L. Hao, J. Chen, W. D. Li, B. B. Wang, X. D. Wang, and W. Becker, *Phys. Rev. Lett.* **112**, 073002 (2014); X. L. Hao, W. D. Li, J. Liu, and J. Chen, *Phys. Rev. A* **83**, 053422 (2011).
  - [15] H. Soifer, P. Botheron, D. Shafir, A. Diner, O. Raz, B. D. Bruner, Y. Mairesse, B. Pons, and N. Dudovich, *Phys. Rev. Lett.* **105**, 143904 (2010).
  - [16] W. H. Xiong, L. Y. Peng, and Q. Gong, *J. Phys. B: At., Mol. Opt. Phys.* **50**, 032001 (2017).
  - [17] M. Klaiber, K. Z. Hatsagortsyan, and C. H. Keitel, *Phys. Rev. Lett.* **114**, 083001 (2015).
  - [18] M. Li, J. W. Geng, M. Han, M. M. Liu, L. Y. Peng, Q. H. Gong, and Y. Q. Liu, *Phys. Rev. A* **93**, 013402 (2016).
  - [19] H. C. Ni, U. Saalmann, and J. M. Rost, *Phys. Rev. A* **97**, 013426 (2018).
  - [20] A. N. Pfeiffer, C. Cirelli, A. S. Landsman, M. Smolarski, D. Dimitrovski, L. B. Madsen, and U. Keller, *Phys. Rev. Lett.* **109**, 083002 (2012).
  - [21] C. Hofmann, A. S. Landsman, C. Cirelli, A. N. Pfeiffer, and U. Keller, *J. Phys. B: At., Mol. Opt. Phys.* **46**, 125601 (2013).
  - [22] R. H. Xu, T. Li, and X. Wang, *Phys. Rev. A* **98**, 053435 (2018).
  - [23] N. Camus, E. Yakaboylu, L. Fechner, M. Klaiber, M. Laux, Y. Mi, K. Z. Hatsagortsyan, T. Pfeifer, C. H. Keitel, and R. Moshhammer, *Phys. Rev. Lett.* **119**, 023201 (2017).
  - [24] N. Teeny, E. Yakaboylu, H. Bauke, and C. H. Keitel, *Phys. Rev. Lett.* **116**, 063003 (2016).
  - [25] M. Li, H. Xie, W. Cao, S. Luo, J. Tan, Y. Feng, B. Du, W. Zhang, Y. Li, Q. Zhang, P. Lan, Y. Zhou, and P. Lu, *Phys. Rev. Lett.* **122**, 183202 (2019).
  - [26] L. Guo, S. S. Han, and J. Chen, *Opt. Express* **18**, 1240 (2010).
  - [27] L. Guo, S. S. Han, and J. Chen, *Phys. Rev. A* **86**, 053409 (2012); L. Guo, S. S. Han, S. L. Hu, and J. Chen, *J. Phys. B: At., Mol. Opt. Phys.* **50**, 125006 (2017); L. Guo *et al.*, [arXiv:1905.00213](https://arxiv.org/abs/1905.00213).
  - [28] L. Guo, M. Q. Liu, R. H. Lu, S. S. Han, and J. Chen, *Laser Part. Beams* **37**, 448 (2019).
  - [29] W. Becker, F. Grasbon, R. Kopold, D. B. Milošević, G. G. Paulus, and H. Walther, *Adv. At. Mol. Opt. Phys.* **48**, 35 (2002).
  - [30] D. B. Milošević and F. Ehlotzky, *Adv. At. Mol. Opt. Phys.* **49**, 373 (2003).
  - [31] H. R. Reiss, *Phys. Rev. A* **22**, 1786 (1980).
  - [32] C. Figueira de Morisson Faria, H. Schomerus, and W. Becker, *Phys. Rev. A* **66**, 043413 (2002).